Determination of QCD phase diagram from the imaginary chemical potential region

Yuji Sakai,[1,*] Kouji Kashiwa,[1,†] Hiroaki Kouno,[2,‡] Masayuki Matsuzaki,[3,§] and Masanobu Yahiro[1,‖]

[1]*Department of Physics, Graduate School of Sciences, Kyushu University, Fukuoka 812-8581, Japan*

[2]*Department of Physics, Saga University, Saga 840-8502, Japan*

[3]*Department of Physics, Fukuoka University of Education, Munakata, Fukuoka 811-4192, Japan*

(Received 4 February 2009; published 1 May 2009)

We test the reliability of the Polyakov-loop extended Nambu–Jona-Lasinio (PNJL) model, comparing the model result with the lattice data at nonzero imaginary chemical potential. The PNJL model with the vector-type four-quark and scalar-type eight-quark interactions reproduces the lattice data on the pseudocritical temperatures of the deconfinement and chiral phase transitions. The QCD phase diagram in the real chemical potential region is predicted by the PNJL model. The critical end point survives, even if the vector-type four-quark interaction is taken into account.

DOI: 10.1103/PhysRevD.79.096001 PACS numbers: 11.30.Rd, 12.40.−y

I. INTRODUCTION

Quantum chromodynamics (QCD) is a remarkable theory. It is renormalizable and essentially parameter free. QCD accounts for the rich phenomenology of hadronic and nuclear physics. Thermodynamics of QCD is also well defined. Nevertheless, it is not well known because of its nonperturbative nature. In particular, the QCD phase diagram is essential for understanding not only natural phenomena such as compact stars and the early universe but also laboratory experiments such as relativistic heavy-ion collisions.

Unfortunately, quantitative calculations of the phase diagram from first-principle lattice QCD (LQCD) have the well-known sign problem when the chemical potential (μ) is real; for example, see Ref. [1] and references therein. So far, several approaches have been proposed to circumvent the difficulty; for example, the reweighting method [2], the Taylor-expansion method [3], and the analytic continuation to real chemical potential (μ_{R}) from imaginary chemical potential (μ_{I}) [4–8]. However, those are still far from perfection.

As an approach complementary to first-principle lattice QCD, we can consider effective models such as the Nambu–Jona-Lasinio (NJL) model [9–17] and the Polyakov-loop extended Nambu–Jona-Lasinio (PNJL) model [18–35]. The NJL model describes the chiral symmetry breaking, but not the confinement mechanism. The PNJL model is designed [20] to make it possible to treat the Polyakov loop as well as the chiral symmetry breaking.

In the NJL-type models, the input parameters are determined at $\mu = 0$ and $T \geq 0$, where T is temperature. It is then highly nontrivial whether the models predict properly dynamics of QCD at finite μ_{R}. This should be tested from QCD. Fortunately, this is possible in the μ_{I} region, since lattice QCD has no sign problem there. The canonical partition function $Z_{\mathrm{C}}(n)$ with real quark number n is the Fourier transform of the grand-canonical one $Z_{\mathrm{GC}}(\theta)$ with $\theta = \mu_{\mathrm{I}}/T$ [36]:

$$Z_{\mathrm{C}}(n) = \frac{1}{2\pi}\int_{-\pi}^{\pi} d\theta e^{-in\theta} Z_{\mathrm{GC}}(\theta). \tag{1}$$

Thus, the thermodynamic potential of QCD, $\Omega_{\mathrm{QCD}}(\theta) = -T\ln(Z_{\mathrm{GC}}(\theta))$, at finite θ includes all dynamics at real n and hence at finite μ_{R} . Therefore, the reliability of effective models at finite μ_{R} can be tested in the μ_{I} region.

Roberge and Weiss found [36] that QCD has a periodicity $\Omega_{\mathrm{QCD}}(\theta) = \Omega_{\mathrm{QCD}}(\theta + 2\pi k/3)$, showing that $\Omega_{\mathrm{QCD}}(\theta + 2\pi k/3)$ is transformed into $\Omega_{\mathrm{QCD}}(\theta)$ by the $\mathbb{Z}_3$ transformation with integer k. This means that QCD is invariant under a combination of the $\mathbb{Z}_3$ transformation and a parameter transformation $\theta \to \theta + 2k\pi/3$ [34–36],

$$\begin{gathered} q \to Uq, \qquad A_\nu \to UA_\nu U^{-1} - i/g(\partial_\nu U)U^{-1}, \\ \theta \to \theta + 2\pi k/3, \end{gathered} \tag{2}$$

where $U(x,\tau)$ are elements of $SU(3)$ with $U(x,\beta = 1/T) = \exp(-2i\pi k/3)U(x,0)$ and q is the quark field. We call this combination the extended $\mathbb{Z}_3$ transformation. Thus, $\Omega_{\mathrm{QCD}}(\theta)$ has the extended $\mathbb{Z}_3$ symmetry, and hence quantities invariant under the extended $\mathbb{Z}_3$ transformation have the Roberge-Weiss (RW) periodicity [34–36] . At the present stage, the PNJL model is only a realistic effective model that possesses both the extended $\mathbb{Z}_3$ symmetry and chiral symmetry [34,35]. This property makes it possible to compare the PNJL model with lattice QCD quantitatively in the μ_{I} region. If the PNJL model succeeds in reproducing the lattice data, we may think that the PNJL model will predict, with high reliability, the QCD phase structure in the μ_{R} region.

*sakai@phys.kyushu-u.ac.jp
†kashiwa@phys.kyushu-u.ac.jp
‡kounoh@cc.saga-u.ac.jp
§matsuza@fukuoka-edu.ac.jp
‖yahiro@phys.kyushu-u.ac.jp

The extended $\mathbb{Z}_3$ symmetry in QCD is a remnant of the $\mathbb{Z}_3$ symmetry, namely the confinement mechanism, in the pure gauge system. The extended $\mathbb{Z}_3$ symmetry appears as the RW periodicity in the $\mu_{\rm I}$ region and implicitly affects dynamics in the $\mu_{\rm R}$ region. Actually, the mechanism largely shifts the critical end point [10] toward higher T and lower μ than the NJL model predicts [21,25,31]. In contrast, the vector-type four-quark interaction $G_{\rm v}(\bar{q}\gamma_\mu q)^2$ largely moves the critical end point in the opposite direction [14,16,21,31], if it is newly added to the NJL and PNJL models. Thus, it is essential to determine the strength of the coupling $G_{\rm v}$ of the vector-type interaction, although the interaction is often ignored in the NJL and PNJL calculations.

In the relativistic meson-nucleon theory [37], the repulsive force mediated by vector mesons is essential to account for the saturation property of nuclear matter. Using the auxiliary field method, one can convert quark-quark interactions to meson-quark interactions; for example, see Refs. [17,38,39] and references therein. In the hadron phase, quarks have a large effective mass as a result of spontaneous chiral symmetry breaking, and then nucleons can be considered to be formed by such three heavy quarks, i.e. three constituent quarks. It is then natural to think that there exists a correspondence between the meson-nucleon interactions and the quark-quark interactions. In this sense, it is very likely that the vector-type four-quark interaction is not negligible and even significant, in particular, at a finite quark-density region corresponding to the nuclear saturation density. In the previous work [35], we have proposed that the strength of $G_{\rm v}$ can be determined from lattice data on the chiral phase transition in the $\mu_{\rm I}$ region.

In this paper, we consider two-flavor QCD and show the reliability of the PNJL model, quantitatively comparing the model result with lattice data in the $\mu_{\rm I}$ region. The model parameters except $G_{\rm v}$ are fixed by the measured pion mass and decay constant at $\mu = T = 0$ and lattice data [40–42] at $T > 0$ and $\mu = 0$. The PNJL calculation with no vector-type interaction well reproduces lattice data [4,8] on the pseudocritical temperature $T_{\rm c}(\Phi)$ of the deconfinement phase transition, but not on the pseudocritical temperature $T_{\rm c}(\sigma)$ of the chiral phase transition near $\theta = \pi/3$. The strength of $G_{\rm v}$ is fitted so as to reproduce the latter data. The primary result of the lattice simulations is that $T_{\rm c}(\Phi)$ coincides with $T_{\rm c}(\sigma)$, within numerical errors, in the entire region of θ [4,8]. The PNJL model with the vector-type interaction can reproduce this property. Finally, we quantitatively predict the phase diagram in the $\mu_{\rm R}$ region by using the PNJL model with the parameter set justified in the $\mu_{\rm I}$ region. These sorts of model predictions are quite important before doing heavy lattice calculations with large lattice size in the $\mu_{\rm I}$ region.

In Sec. II, the PNJL model is explained simply. In Sec. III, we test the PNJL model in the $\mu_{\rm I}$ region and determine the strength of $G_{\rm v}$. Finally, we predict the phase diagram in the $\mu_{\rm R}$ region. Section IV is devoted to a summary.

II. PNJL MODEL

The two-flavor PNJL Lagrangian is

$$\mathcal{L} = \bar{q}(i\gamma_\nu D^\nu - m_0)q + G_{\rm s}[(\bar{q}q)^2 + (\bar{q}i\gamma_5\vec{\tau}q)^2] - \mathcal{U}(\Phi[A], \Phi[A]^*, T), \tag{3}$$

where q denotes the two-flavor quark field, m_0 does the current quark mass, and $D^\nu = \partial^\nu + iA^\nu - i\mu\delta^\nu_0$. The field A^ν is defined as $A^\nu = \delta^\nu_0 g A^0_a \frac{\lambda^a}{2}$ with the gauge field A^ν_a, the Gell-Mann matrix λ_a, and the gauge coupling g. In the NJL sector, $G_{\rm s}$ denotes the coupling constant of the scalar-type four-quark interaction. Later, we will add the vector-type four-quark interaction [10,14,16,35] and the scalar-type eight-quark interaction [15,16,34] to the PNJL Lagrangian. The Polyakov potential $\mathcal{U}$, defined in (10), is a function of the Polyakov loop Φ and its Hermitian conjugate Φ^*,

$$\Phi = \frac{1}{N_{\rm c}}{\rm Tr}L, \qquad \Phi^* = \frac{1}{N_{\rm c}}{\rm Tr}L^\dagger, \tag{4}$$

with

$$L(\mathbf{x}) = \mathcal{P}\exp\left[i\int_0^\beta d\tau A_4(\mathbf{x},\tau)\right], \tag{5}$$

where $\mathcal{P}$ is the path ordering and $A_4 = iA_0$. In the chiral limit ($m_0 = 0$), the Lagrangian density has the exact $SU(N_f)_{\rm L} \times SU(N_f)_{\rm R} \times U(1)_{\rm v} \times SU(3)_{\rm c}$ symmetry.

The temporal component of the gauge field is diagonal in the flavor space, because the color and the flavor space are completely separated out in the present case. In the Polyakov gauge, L can be written in a diagonal form in the color space [20]:

$$L = e^{i\beta(\phi_3\lambda_3 + \phi_8\lambda_8)} = {\rm diag}(e^{i\beta\phi_a}, e^{i\beta\phi_b}, e^{i\beta\phi_c}), \tag{6}$$

where $\phi_a = \phi_3 + \phi_8/\sqrt{3}$, $\phi_b = -\phi_3 + \phi_8/\sqrt{3}$, and $\phi_c = -(\phi_a + \phi_b) = -2\phi_8/\sqrt{3}$. The Polyakov loop Φ is an exact order parameter of the spontaneous $\mathbb{Z}_3$ symmetry breaking in the pure gauge theory. Although the $\mathbb{Z}_3$ symmetry is not an exact one in the system with dynamical quarks, it still seems to be a good indicator of the deconfinement phase transition. Therefore, we use Φ to define the deconfinement phase transition.

Making the mean field approximation and performing the path integral over quark field, one can obtain the thermodynamic potential Ω (per unit volume),

$$\Omega = -2N_f \int \frac{d^3\mathrm{p}}{(2\pi)^3}\Big[3E(\mathrm{p}) + \frac{1}{\beta}\ln[1+3(\Phi+\Phi^* e^{-\beta E^-(\mathrm{p})})e^{-\beta E^-(\mathrm{p})} + e^{-3\beta E^-(\mathrm{p})}] + \frac{1}{\beta}\ln[1+3(\Phi^*+\Phi e^{-\beta E^+(\mathrm{p})})e^{-\beta E^+(\mathrm{p})} + e^{-3\beta E^+(\mathrm{p})}]\Big] + U_{\mathrm{M}} + \mathcal{U}, \quad (7)$$

where $\sigma = \langle\bar{q}q\rangle$, $\Sigma_{\mathrm{s}} = -2G_{\mathrm{s}}\sigma$, $M = m_0 + \Sigma_{\mathrm{s}}$, $U_{\mathrm{M}} = G_{\mathrm{s}}\sigma^2$, $E(\mathrm{p}) = \sqrt{\mathbf{p}^2 + M^2}$, and $E^{\pm}(\mathrm{p}) = E(\mathrm{p}) \pm \mu = E(\mathrm{p}) \pm i\theta/\beta$. In (7), only the first term of the right-hand side diverges. It is then regularized by the three-dimensional momentum cutoff Λ [20,24]. We use $\mathcal{U}$ of Ref. [25] that is fitted to a lattice QCD simulation in the pure gauge theory at finite T [43,44]:

$$\mathcal{U} = T^4\Big[-\frac{a(T)}{2}\Phi^*\Phi + b(T) \times \ln(1 - 6\Phi\Phi^* + 4(\Phi^3 + \Phi^{*3}) - 3(\Phi\Phi^*)^2)\Big], \quad (8)$$

$$a(T) = a_0 + a_1\Big(\frac{T_0}{T}\Big) + a_2\Big(\frac{T_0}{T}\Big)^2, \qquad b(T) = b_3\Big(\frac{T_0}{T}\Big)^3, \quad (9)$$

where parameters are summarized in Table I. The Polyakov potential yields a first-order deconfinement phase transition at $T = T_0$ in the pure gauge theory. The original value of T_0 is 270 MeV evaluated by the pure gauge lattice QCD calculation. However, the PNJL model with this value of T_0 yields a somewhat larger value of the transition temperature at zero chemical potential than the full LQCD simulation [40–42] predicts. Therefore, we rescale T_0 to 212 MeV; the detail will be shown in Sec. III A.

The variables $X = \Phi$, Φ^*, and σ satisfy the stationary conditions,

$$\partial\Omega/\partial X = 0. \quad (10)$$

The solutions of the stationary conditions do not give the global minimum Ω necessarily. There is a possibility that they yield a local minimum or even a maximum. We then have checked that the solutions yield the global minimum when the solutions $X(\theta)$ are inserted into (7).

The thermodynamic potential Ω of Eq. (7) is not invariant under the $\mathbb{Z}_3$ transformation,

$$\Phi(\theta) \to \Phi(\theta)e^{-i2\pi k/3}, \qquad \Phi(\theta)^* \to \Phi(\theta)^* e^{i2\pi k/3}, \quad (11)$$

TABLE I. Summary of the parameter set in the Polyakov sector used in Ref. [25]. All parameters are dimensionless.

a_0	a_1	a_2	b_3
3.51	−2.47	15.2	−1.75

although $\mathcal{U}$ of (8) is invariant. Instead of the $\mathbb{Z}_3$ symmetry, however, Ω is invariant under the extended $\mathbb{Z}_3$ transformation,

$$e^{\pm i\theta} \to e^{\pm i\theta}e^{\pm i(2\pi k/3)}, \qquad \Phi(\theta) \to \Phi(\theta)e^{-i(2\pi k/3)}, \qquad \Phi(\theta)^* \to \Phi(\theta)^* e^{i(2\pi k/3)}. \quad (12)$$

This is easily understood as follows. It is convenient to introduce the modified Polyakov loop $\Psi \equiv e^{i\theta}\Phi$ and $\Psi^* \equiv e^{-i\theta}\Phi^*$ invariant under the transformation (12). The extended $\mathbb{Z}_3$ transformation is then rewritten into

$$e^{\pm i\theta} \to e^{\pm i\theta}e^{\pm i(2\pi k/3)}, \qquad \Psi(\theta) \to \Psi(\theta), \qquad \Psi(\theta)^* \to \Psi(\theta)^*, \quad (13)$$

and Ω is also into

$$\Omega = -2N_f \int \frac{d^3\mathrm{p}}{(2\pi)^3}\Big[3E(\mathrm{p}) + \frac{1}{\beta}\ln[1 + 3\Psi e^{-\beta E(\mathrm{p})} + 3\Psi^* e^{-2\beta E(\mathrm{p})}e^{\beta\mu_{\mathrm{B}}} + e^{-3\beta E(\mathrm{p})}e^{\beta\mu_{\mathrm{B}}}] + \frac{1}{\beta}\ln[1 + 3\Psi^* e^{-\beta E(\mathrm{p})} + 3\Psi e^{-2\beta E(\mathrm{p})}e^{-\beta\mu_{\mathrm{B}}} + e^{-3\beta E(\mathrm{p})}e^{-\beta\mu_{\mathrm{B}}}]\Big] + U_{\mathrm{M}} + \mathcal{U}, \quad (14)$$

where $\beta\mu_{\mathrm{B}} = 3\beta\mu = 3i\theta$. Obviously, Ω is invariant under the extended $\mathbb{Z}_3$ transformation (13), since it is a function of only extended $\mathbb{Z}_3$ invariant quantities, $e^{3i\theta}$ and $\tilde{X}(= \Psi, \Psi^*, \sigma)$. The explicit θ dependence appears only through the factor $e^{3i\theta}$ in (14). Hence, the stationary conditions (10) show that $\tilde{X} = \tilde{X}(e^{3i\theta})$. Inserting the solutions back to (14), one can see that $\Omega = \Omega(e^{3i\theta})$. Thus, $\tilde{X}$ and Ω have the RW periodicity,

$$\tilde{X}\Big(\theta + \frac{2\pi k}{3}\Big) = \tilde{X}(\theta), \quad \text{and} \quad \Omega\Big(\theta + \frac{2\pi k}{3}\Big) = \Omega(\theta), \quad (15)$$

while the Polyakov loop Φ and its Hermitian conjugate Φ^* have the properties

$$\Phi\Big(\theta + \frac{2\pi k}{3}\Big) = e^{-i2\pi k/3}\Phi(\theta), \qquad \Phi\Big(\theta + \frac{2\pi k}{3}\Big)^* = e^{i2\pi k/3}\Phi(\theta)^*. \quad (16)$$

III. NUMERICAL RESULTS

A. Thermal system with no chemical potential

First, we consider the thermal system with no chemical potential to determine the parameters, m_0, G_{s}, Λ, and T_0, of the PNJL model. In the lattice calculations [40–42], the pseudocritical temperature $T_{\mathrm{c}}(\sigma)$ of the crossover chiral phase transition coincides with that $T_{\mathrm{c}}(\Phi)$ of the crossover deconfinement one within 10% error: $T_{\mathrm{c}}(\sigma) \approx T_{\mathrm{c}}(\Phi) \approx 173 \pm 8$ MeV [41].

TABLE II. Summary of the parameter sets in the PNJL calculations. The parameters Λ, m_0, and T_0 are common among the three sets; $\Lambda = 631.5$ MeV, $m_0 = 5.5$ MeV, and $T_0 = 212$ MeV.

Set	G_s	G_{s8}	G_v
A	5.498 GeV^{-2}	0	0
B	4.673 GeV^{-2}	452.12 GeV^{-8}	0
C	4.673 GeV^{-2}	452.12 GeV^{-8}	4.673 GeV^{-2}

The parameter set, $\Lambda = 631.5$ MeV, $G_s = 5.498$ [GeV^{-2}], and $m_0 = 5.5$ MeV, can reproduce the pion decay constant $f_\pi = 93.3$ MeV and the pion mass $M_\pi = 138$ MeV at $T = \mu = 0$ [16], and keeps a good reproduction also at finite T [25]. We then adopt these values for Λ, G_s , and m_0. We adjust T_0 so that the PNJL calculation can reproduce the lattice result $T_c(\Phi) = 173$ MeV; the value is $T_0 = 212$ MeV. The parameter set thus determined is shown as set A in Table II.

Figure 1 shows the chiral condensate σ normalized by $\sigma_0 = \sigma|_{T=0,\mu=0}$ and the absolute value of the Polyakov loop Φ as a function of T/T_c. In this paper T_c is always taken to be 173 MeV. The thin curves represent the PNJL results of parameter set A, where $\sigma_0 = -0.0302$ [GeV^3] in this case. Lattice QCD data [40–42] are also plotted by cross symbols with a 10% error bar; σ and $|\Phi|$ measured as a function of T/T_c in Refs. [40–42] have only small errors, but we have added 10% error that the lattice calculation [41] has in determining T_c . For $|\Phi|$ the PNJL result (thin solid curve) reasonably agrees with the lattice one ($\times$). For σ, however, the PNJL result (thin dashed curve) considerably overshoots the lattice data (+).

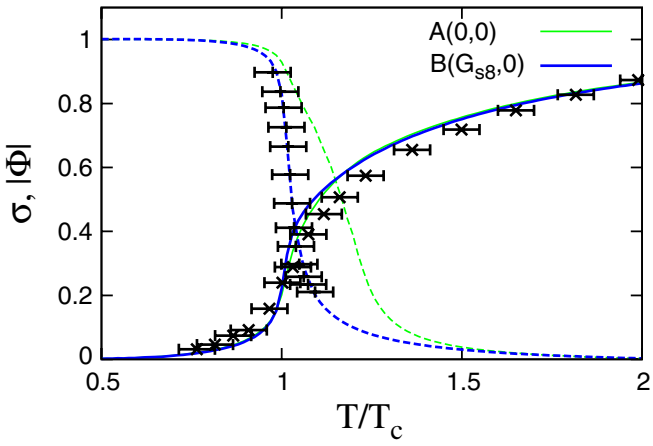

FIG. 1 (color online). Chiral condensate σ normalized by $\sigma(T = 0, \mu = 0)$ and the absolute value of the Polyakov loop Φ. The thick (thin) curves represent the PNJL result of parameter set B (A) with (without) the scalar-type eight-quark interaction; σ ($|\Phi|$) is denoted by the dashed (solid) curves. Lattice data (+) on σ are taken from Ref. [40] and those ($\times$) on $|\Phi|$ are from Ref. [42]. The lattice data are plotted with a 10% error bar, since lattice calculations have 10% error in determining T_c [41].

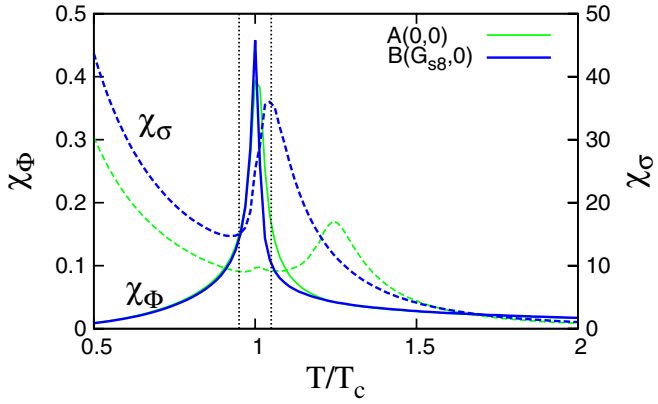

FIG. 2 (color online). T dependence of chiral and Polyakov-loop susceptibilities, χ_σ (right scale) and χ_Φ (left scale). The thick (thin) curves represent the PNJL result of parameter set B (A) with (without) the scalar-type eight-quark interaction; χ_σ (χ_Φ) is denoted by the dashed (solid) curves. The region between two vertical dotted lines $T = (1 \pm 0.05)T_c$ is the prediction of lattice calculations [41].

Figure 2 represents results of the PNJL calculations for chiral and Polyakov-loop susceptibilities, χ_σ and χ_Φ [21]. Peak positions of χ_σ and χ_Φ show $T_c(\sigma)$ and $T_c(\Phi)$, respectively. The PNJL results (thin curves) of parameter set A give $T_c(\sigma)/T_c = 1.25$ and $T_c(\Phi)/T_c = 1$, while the lattice simulations yield $T_c(\sigma)/T_c = 1 \pm 0.05$ and $T_c(\Phi)/T_c = 1 \pm 0.05$. The PNJL results are consistent with the lattice ones for $T_c(\Phi)$, but not for $T_c(\sigma)$.

Now we introduce the scalar-type eight-quark interaction [16],

$$G_{s8}[(\bar{q}q)^2 + (\bar{q}i\gamma_5\vec{\tau}q)^2]^2, \tag{17}$$

since the difference $T_c(\sigma) - T_c(\Phi)$ is reduced by the interaction [34].

Since f_π and M_π calculated with PNJL depend on the strength of G_{s8}, for each value of G_{s8} the strength of G_s is readjusted so as to reproduce the measured values $f_\pi = 93.3$ MeV and $M_\pi = 138$ MeV. As G_{s8} increases from zero, $T_c(\sigma)$ calculated with PNJL decreases toward $T_c = 173$ MeV. When $G_{s8} = 452.12$ GeV^{-8}, the ratio $T_c(\sigma)/T_c$ becomes 1.05 and, hence, is consistent with the corresponding lattice result within 10% error. We adopt this strength. This parameter set is shown as set B in Table II. As shown in Fig. 1, the PNJL results (thick curves) of parameter set B well reproduce the lattice results for both the chiral condensate and the Polyakov loop.

B. Thermal system with imaginary chemical potential

In this subsection, we consider the thermal system with finite imaginary chemical potential and compare the PNJL result with the lattice data [4,8] in which the lattice size is $8^3 \times 4$ and the two-flavor Kogut-Susskind and Wilson fermions are considered.

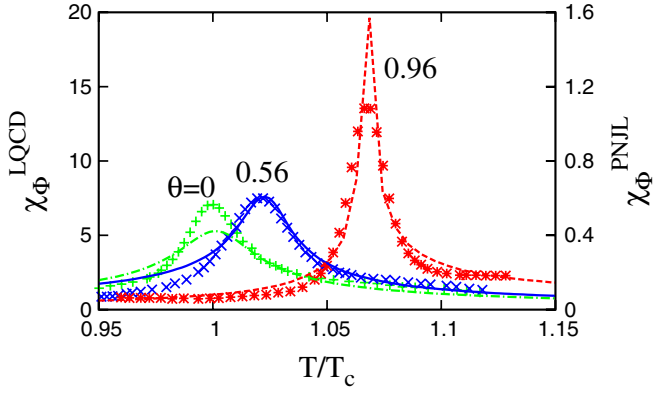

FIG. 3 (color online). T dependence of the Polyakov-loop susceptibilities in three cases of $\theta = 0$, 0.56, and 0.96. Curves represent the PNJL results of set A (right scale). Lattice data shown by crosses (left scale) are taken from Ref. [8].

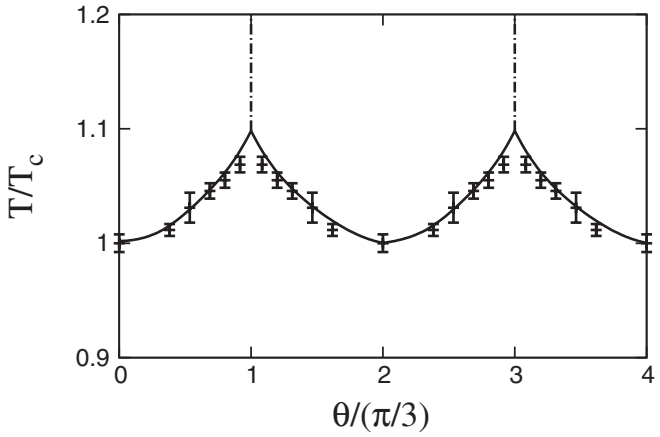

FIG. 4. Phase diagram on the θ-T plane. The solid curve represents the deconfinement phase transition, while the dot-dashed lines do the RW phase transition predicted by the PNJL calculation with set A. Lattice data are taken from Ref. [8].

First, we analyze the deconfinement phase transition. Since the eight-quark interaction hardly changes the Polyakov loop, we do the PNJL calculation with the parameter set A. Figure 3 presents T dependence of the Polyakov-loop susceptibility χ_Φ in three cases of $\theta = 0$, 0.56, and 0.96. For each θ, the PNJL result (curve) reproduces the corresponding lattice result (crosses) in its peak position. Thus, the PNJL results are consistent with the lattice ones for the pseudocritical temperature of the crossover deconfinement phase transition.

Figure 4 presents the phase diagram of the deconfinement phase transition in the θ-T plane, where θ is divided by $\pi/3$ and T is normalized by $T_c = 173$ MeV. Lattice data [8] measured as a function of T/T_c have only small errors, as shown by thick error bars in Fig. 4. This is an error bar in the case that lattice calculations have no error in T_c. However, the lattice calculation [41] has about 10% error in determining T_c, as mentioned in Sec. III A. This 10% error should be added to the original small error; this 10% error will be shown later in Fig. 6. The PNJL result (solid curve) of set A agrees with the lattice one (crosses) within the error bars. The phase diagram has a periodicity of $2\pi/3$ in θ. This is called the RW periodicity [36]. The phase diagram is also θ even, because so is χ_Φ. On the dot-dashed line going up from an end point $(\theta_{\rm RW}, T_{\rm RW}) = (\pi/3, 1.09T_c)$, the quark-number density n and the phase ϕ of the Polyakov loop are discontinuous in the PNJL calculations [34,35]. This is called the RW phase transition line. The lattice data [4,8] on ϕ are also discontinuous on the line, as shown later in Fig. 7. Thus, the PNJL result is consistent with the lattice results [4,8] also for the location of the RW phase transition line.

The lattice simulations [4,8] point out that $T_c(\sigma)$ agrees with $T_c(\Phi)$ within numerical errors in the entire region $0 \le \theta \le 2\pi/3$. We then take the case of $\theta = \pi/3$ to consider this point. It is predicted by the lattice simulations that $T_c(\sigma)$ and $T_c(\Phi)$ are located in the region between two

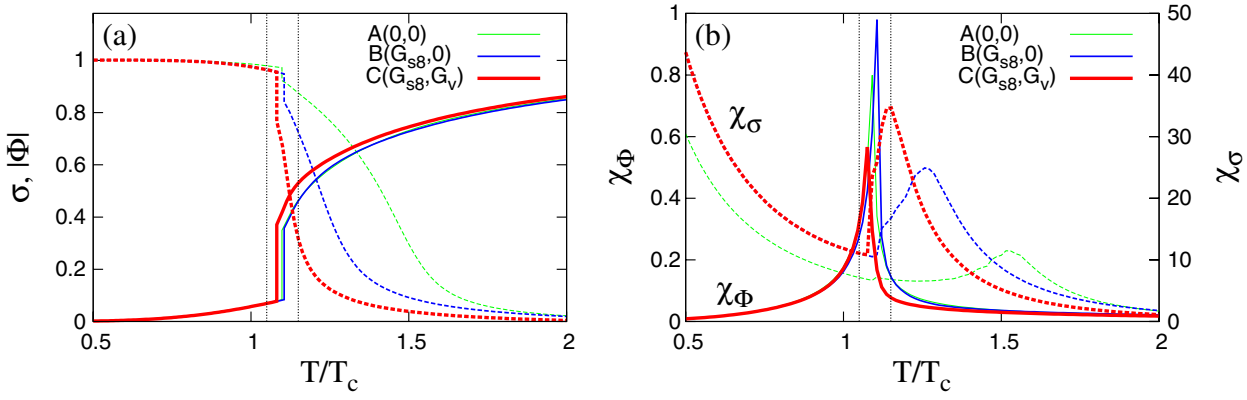

FIG. 5 (color online). T dependence of (a) the normalized chiral condensate and the absolute value of the Polyakov loop and (b) the susceptibilities χ_σ (right scale) and χ_Φ (left scale) at $\theta = \pi/3$. In panel (a), σ ($|\Phi|$) is denoted by the dashed (solid) curves. In panel (b), χ_σ (χ_Φ) is denoted by the dashed (solid) curves. The PNJL calculations are done with three parameter sets of A, B, and C. The region between two vertical dotted lines $T = (1.1 \pm 0.05)T_c$ is the prediction of $T_{\rm RW}$ by the lattice calculations [4,8].

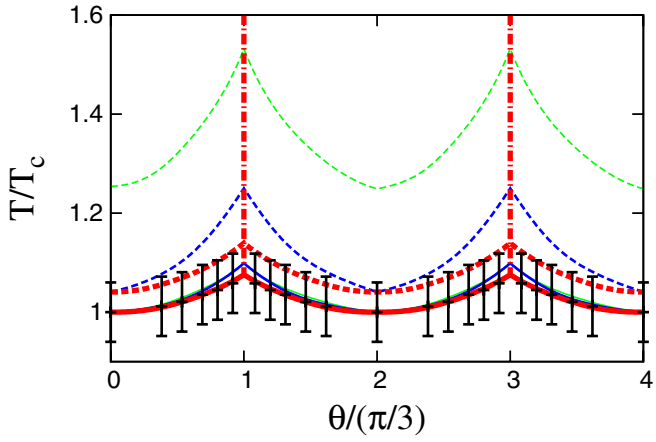

FIG. 6 (color online). Phase diagrams of the chiral phase transition in the imaginary chemical potential region calculated with three parameter sets are presented by dashed curves; thin, thick, and bold ones are results of the PNJL calculations with set A, B, and C, respectively. Lattice data [8] are shown with 10% error that T_c has [41]. The deconfinement phase transition curve (bold solid curve) and the RW phase transition lines (bold dot-dashed lines) calculated with set C are also shown for comparison.

vertical dotted lines of Fig. 5. Panel (a) shows σ and $|\Phi|$ as a function of T/T_c and panel (b) does χ_σ and χ_Φ as a function of T/T_c. The thin (thick) curves represent results of the PNJL calculations with set A (B). The eight-quark interaction hardly shifts the peak position of χ_Φ, i.e. $T_c(\Phi)$, from the value $1.09T_c$. The peak position is consistent with the lattice result shown by the region between two vertical dotted lines. In contrast, the eight-quark interaction largely shifts the peak position of χ_σ, i.e. $T_c(\sigma)$, from $1.53T_c$ to $1.24T_c$, but the shifted value still deviates from $T_c(\Phi) = (1.1 \pm 0.05)T_c$, that is, the lattice data near $\theta = \pi/3$ [4,8] shown by the region between two vertical dotted lines.

In order to solve this problem, we introduce the vector-type four-quark interaction

$$-G_v(\bar{q}\gamma_\mu q)^2 \tag{18}$$

and add it to the PNJL Lagrangian $\mathcal{L}$; see Ref. [35] for the detail of this formulation. As mentioned in Ref. [35], the phase structure in the real chemical potential region is quite sensitive to the strength of the coupling G_v. It is then important to determine the strength, but it has not been done yet. Since the vector-type interaction does not change the pion mass and the pion decay constant at $T = \mu = 0$ and the chiral condensate and the Polyakov loop at $T \geq 0$ and $\mu = 0$, we can simply add the interaction to set B. As G_v increases from zero, $T_c(\sigma)$ goes down toward $T_c(\Phi)$, while $T_c(\Phi)$ moves little. When $G_v = 4.673\ \mathrm{GeV}^{-2}$, $T_c(\sigma)$ gets into the region between the vertical dotted lines. We adopt this strength of G_v. This set is shown as set C in Table II.

When this value of G_v is taken, the omega meson mass at $\mu = 0$ and $T = 0$ estimated by the Bethe-Salpeter formalism [45] is about 695 MeV and then 11% smaller than the measured value 782 MeV. This difference may be related to the fact that the omega meson mass is larger than the cutoff $\Lambda = 631.5$ MeV we use. At present, thus, the calculation of the vector meson mass is beyond our scope, but this problem is interesting as a future work.

Figure 6 shows the phase diagram of the chiral phase transition determined by $T_c(\sigma)$. Thin, thick, and bold curves are results of the PNJL calculations with sets A, B, and C, respectively. In the entire region $0 \leq \theta \leq 2\pi/3$, the eight-quark interaction moves $T_c(\sigma)$ down from the thin dashed curve (set A) to the thick one (set B). However, the thick dashed curve still overshoots the lattice result (symbols) with 10% error near $\theta = \pi/3$. The vector-type interaction makes the thick dashed curve go down to the bold one (set C) that is consistent with the lattice result [8]. Thus, the PNJL calculations with set C can reproduce the

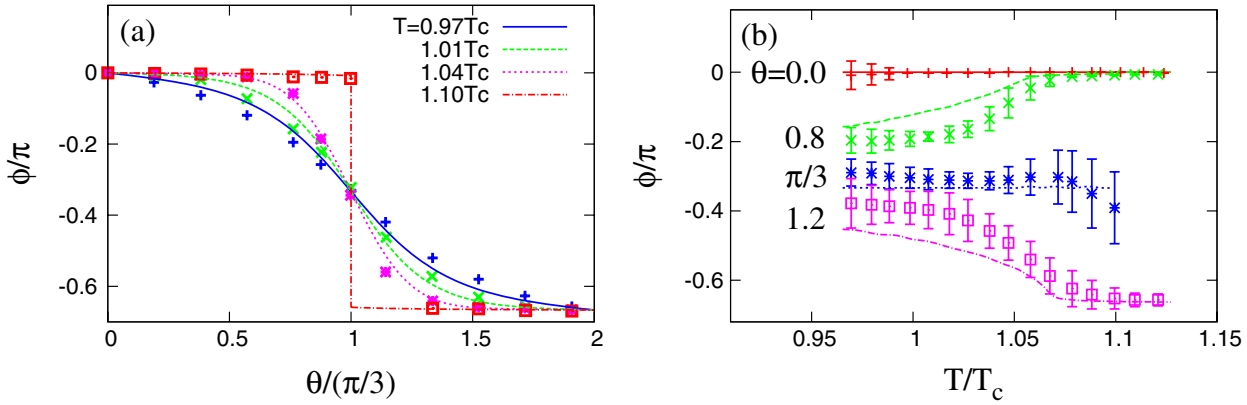

FIG. 7 (color online). Phase ϕ of the Polyakov loop as a function of (a) θ and (b) T. Lattice data [4,8] are plotted by symbols. Curves represent results of PNJL calculations with set A. In panel (b), four cases (solid, dashed, dotted, and dot-dashed) from top to bottom represent results of $\theta = 0$, 0.8, $\pi/3$, and 1.2, respectively. The dotted line terminates at $T = T_{RW} = 1.09T_c$, since ϕ is singular at $T > T_{RW}$ in the case of $\theta = \pi/3$.

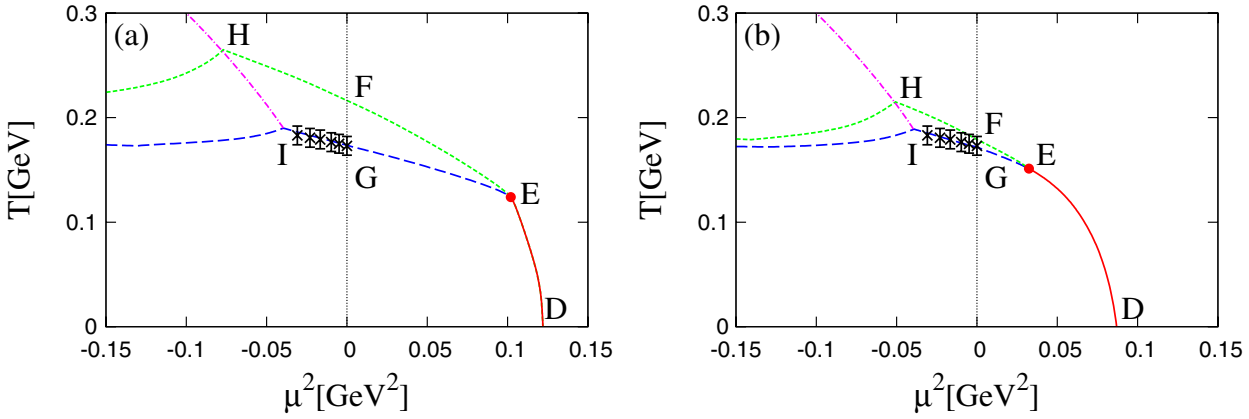

FIG. 8 (color online). Phase diagram in the real and imaginary chemical potential region. Panels (a) and (b) are calculated with the parameter sets A and B, respectively. Cross symbols with error bars indicate the lattice data taken from Ref. [8]. Points D–I are explained in the text.

lattice result [4,8] that $T_c(\sigma)$ coincides with $T_c(\Phi)$ within numerical errors in the entire region $0 \le \theta \le 2\pi/3$.

Figure 7(a) shows θ dependence of the phase ϕ of Φ for four cases of $T/T_c = 0.97$, 1.01, 1.04, and 1.10. The PNJL results (curves) well reproduce the lattice data [4,8] (symbols). It is found from both results that ϕ is continuous at $\theta = \pi/3$ in the low-T side $T \le T_{RW} = 1.09T_c$, but it is discontinuous at $\theta = \pi/3$ in the high-T side $T > T_{RW}$. Hence, the RW phase transition takes place at $T > T_{RW} = 1.09T_c$ and $\theta = \pi/3$.

Figure 7(b) shows T dependence of ϕ for four cases of $\theta = 0$, 0.8, $\pi/3$, and 1.2. The PNJL results (curves) well reproduce the lattice data [4,8] (symbols). For $\theta < \pi/3$ the phase ϕ tends to zero as T increases, while for $\theta > \pi/3$ it does to $-2\pi/3$ as T increases. When $\theta = \pi/3$, the RW phase transition takes place at $T > T_{RW} = 1.09T_c$ and then the phase ϕ is singular there, so that the dotted line terminates at $T = T_{RW}$. In the high-T limit, the region (I) $-\pi/3 < \theta < \pi/3$ has $\phi = 0$ and the region (II) $\pi/3 < \theta < \pi$ does $\phi = -2\pi/3$. Thus, the region (II) is a $\mathbb{Z}_3$ image of the region (I), and the region (III) $\pi < \theta < 5\pi/3$ is another $\mathbb{Z}_3$ image of the region (I).

C. Thermal system with real chemical potential

In this subsection, we predict the phase diagram in the real μ region by using the PNJL model. Figures 8(a) and 8(b) represent the phase diagrams in the μ^2-T plane predicted by the PNJL calculations with parameter sets A and B, respectively. On the solid curve between points E and D, both the first-order chiral and deconfinement phase transitions take place simultaneously, and hence point E is the critical end point of these phase transitions. The dot-dashed curve moving up from point I represents the RW phase transition of first order, and then point I is the critical end point of the RW phase transition. The dashed curve between points H and E means the crossover chiral phase transition, while the long-dashed curve between points I and E does the crossover deconfinement phase transition. Point F (G) is a crossing point between the dashed (long-dashed) curve and the $\mu = 0$ line. Cross symbols with error bars indicate LQCD data [4,8]. The PNJL results with parameter sets A and B are not consistent with the LQCD data in the $\mu^2 < 0$ region. The difference between panels (a) and (b) comes from the effect of the scalar-type eight-quark interaction.

Figure 9 represents the result of the PNJL calculation with parameter set C. This figure is most reliable, since the PNJL result is consistent with the LQCD one [4,8] in the $\mu^2 < 0$ region. Comparing Figs. 8 and 9, one can see that the scalar-type eight-quark interaction and the vector-type four-quark interaction give sizable effects on the phase structure. In particular for the critical end point E, the eight-quark interaction shifts point E to larger T and smaller μ, and the vector-type interaction moves it in the

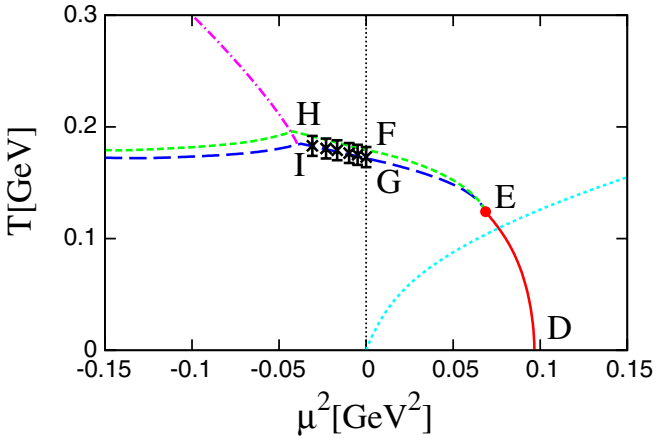

FIG. 9 (color online). Phase diagram in the real and imaginary chemical potential region calculated with the parameter set C. The meaning of the curves and symbols is the same as in Fig. 8, except for the dotted curve starting from the origin, which is explained in the text.

TABLE III. Positions of points D–I in the μ-T plane. The positions of these points are normalized as $(\mu/T_c, T/T_c)$ with $T_c = 173$ MeV.

Set	D	E	F	G	H	I
A	(2.02, 0.00)	(1.84, 0.72)	(0.00, 1.25)	(0.00, 1.00)	$(i\pi/3 \times 1.53, 1.53)$	$(i\pi/3 \times 1.09, 1.09)$
B	(1.68, 0.00)	(1.02, 0.87)	(0.00, 1.05)	(0.00, 1.00)	$(i\pi/3 \times 1.24, 1.24)$	$(i\pi/3 \times 1.09, 1.09)$
C	(1.80, 0.00)	(1.51, 0.72)	(0.00, 1.05)	(0.00, 1.00)	$(i\pi/3 \times 1.13, 1.13)$	$(i\pi/3 \times 1.07, 1.07)$

opposite direction. Positions of points D–I are summarized in Table III.

Recently, progress was made by Ejiri [46] in LQCD simulations. He succeeded in calculating the canonical partition function with reasonable accuracy, using the saddle-point and the Taylor-expansion method allowed for low quark-number density. He constructed the effective potential as a function of the quark-number density and showed that the first-order phase transitions appear in the region $\mu/T > 2.5$. This indicates that the position (μ_E, T_E) of point E is located on a curve $\mu_E/T_E \sim 2.5$. The prediction curve $\mu_E/T_E = 2.5$ is presented by the dotted curve in Fig. 9. The position of point E in the case of parameter set C is consistent with the LQCD prediction.

IV. SUMMARY

We have tested the reliability of the PNJL model, comparing the model result with lattice data in the imaginary chemical potential ($\mu_I = T\theta$) region. In this test, the model parameters except G_v are adjusted so as to reproduce the measured pion mass and decay constant at $T = \mu = 0$ and lattice data [40–42] at $T > 0$ and $\mu = 0$. In this step the eight-quark interaction plays an important role to make $T_c(\sigma)$ closer to $T_c(\Phi)$ as discussed in our previous work [34]. With the aid of this, the PNJL calculation with the eight-quark interaction but without the vector-type interaction well reproduces the lattice data [4,8] at finite θ on Φ and $T_c(\Phi)$, but not on $T_c(\sigma)$ particularly near $\theta = \pi/3$ fully. The strength of G_v is then fitted so as to reproduce the data on $T_c(\sigma)$ near $\theta = \pi/3$. The primary result of the lattice simulations is that $T_c(\Phi)$ coincides with $T_c(\sigma)$, within numerical errors, in the entire region of θ [4,8]. The PNJL model with the eight-quark and vector-type interactions can reproduce this property. Therefore, we can expect that the PNJL model with this parameter set is reliable also in the μ_R region.

Finally, we quantitatively predict the phase diagram in the μ_R region by using the PNJL model with the parameter set mentioned above. The critical end point does not disappear in virtue of the eight-quark interaction, even if the vector-type interaction is taken into account. This is the primary result of the present work. The lattice calculations at nonzero μ_I have small lattice size $(8^3 \times 4)$ [4,8]. Therefore, it is highly expected that lattice simulations with larger size will be done in the μ_I region.

ACKNOWLEDGMENTS

The authors thank A. Nakamura for useful discussions and suggestions. K. K. and H. K. also thank M. Imachi, H. Yoneyama, and M. Tachibana for useful discussions. This work has been supported in part by the Grants-in-Aid for Scientific Research (18540280) of Education, Science, Sports, and Culture of Japan.

[1] J. B. Kogut and D. K. Sinclair, Phys. Rev. D **77**, 114503 (2008).
[2] Z. Fodor and S. D. Katz, Phys. Lett. B **534**, 87 (2002); J. High Energy Phys. 03 (2002) 014.
[3] C. R. Allton, S. Ejiri, S. J. Hands, O. Kaczmarek, F. Karsch, E. Laermann, Ch. Schmidt, and L. Scorzato, Phys. Rev. D **66**, 074507 (2002); S. Ejiri, C. R. Allton, S. J. Hands, O. Kaczmarek, F. Karsch, E. Laermann, and C. Schmidt, Prog. Theor. Phys. Suppl. **153**, 118 (2004).
[4] P. de Forcrand and O. Philipsen, Nucl. Phys. **B642**, 290 (2002).
[5] P. de Forcrand and O. Philipsen, Nucl. Phys. **B673**, 170 (2003).
[6] M. D'Elia and M. P. Lombardo, Phys. Rev. D **67**, 014505 (2003); **70**, 074509 (2004); M. D'Elia, F. D. Renzo, and M. P. Lombardo, Phys. Rev. D **76**, 114509 (2007).
[7] H. S. Chen and X. Q. Luo, Phys. Rev. D **72**, 034504 (2005); arXiv:hep-lat/0702025.
[8] L. K. Wu, X. Q. Luo, and H. S. Chen, Phys. Rev. D **76**, 034505 (2007).
[9] Y. Nambu and G. Jona-Lasinio, Phys. Rev. **122**, 345 (1961); **124**, 246 (1961).
[10] M. Asakawa and K. Yazaki, Nucl. Phys. **A504**, 668 (1989).
[11] J. Berges and K. Rajagopal, Nucl. Phys. **B538**, 215 (1999).
[12] O. Scavenius, Á. Mócsy, I. N. Mishustin, and D. H. Rischke, Phys. Rev. C **64**, 045202 (2001).
[13] H. Fujii, Phys. Rev. D **67**, 094018 (2003).

[14] M. Kitazawa, T. Koide, T. Kunihiro, and Y. Nemoto, Prog. Theor. Phys. **108**, 929 (2002).
[15] A. A. Osipov, B. Hiller, and J. da Providência, Phys. Lett. B **634**, 48 (2006); A. A. Osipov, B. Hiller, J. Moreira, and A. H. Blin, Eur. Phys. J. C **46**, 225 (2006); A. A. Osipov, B. Hiller, J. Moreira, A. H. Blin, and J. da Providência, Phys. Lett. B **646**, 91 (2007); A. A. Osipov, B. Hiller, J. Moreira, and A. H. Blin, Phys. Lett. B **659**, 270 (2008); B. Hiller, A. A. Osipov, A. H. Blin, and J. da Providência, arXiv:0802.3193; B. Hiller, A. A. Osipov, J. Moreira, and A. H. Blin, arXiv:0809.2515; B. Hiller, J. Moreira, A. A. Osipov, and A. H. Blin, arXiv:0812.1532.
[16] K. Kashiwa, H. Kouno, T. Sakaguchi, M. Matsuzaki, and M. Yahiro, Phys. Lett. B **647**, 446 (2007); K. Kashiwa, M. Matsuzaki, H. Kouno, and M. Yahiro, Phys. Lett. B **657**, 143 (2007).
[17] T. Sakaguchi, K. Kashiwa, M. Matsuzaki, H. Kouno, and M. Yahiro, Central Eur. J. Phys. **6**, 116 (2008).
[18] P. N. Meisinger, and M. C. Ogilvie, Phys. Lett. B **379**, 163 (1996).
[19] A. Dumitru and R. D. Pisarski, Phys. Rev. D **66**, 096003 (2002); A. Dumitru, Y. Hatta, J. Lenaghan, K. Orginos, and R. D. Pisarski, Phys. Rev. D **70**, 034511 (2004); A. Dumitru, R. D. Pisarski, and D. Zschiesche, Phys. Rev. D **72**, 065008 (2005).
[20] K. Fukushima, Phys. Lett. B **591**, 277 (2004).
[21] K. Fukushima, Phys. Rev. D **77**, 114028 (2008).
[22] S. K. Ghosh, T. K. Mukherjee, M. G. Mustafa, and R. Ray, Phys. Rev. D **73**, 114007 (2006).
[23] E. Megías, E. R. Arriola, and L. L. Salcedo, Phys. Rev. D **74**, 065005 (2006).
[24] C. Ratti, M. A. Thaler, and W. Weise, Phys. Rev. D **73**, 014019 (2006); C. Ratti, S. Rößner, M. A. Thaler, and W. Weise, Eur. Phys. J. C **49**, 213 (2007).
[25] S. Rößner, C. Ratti, and W. Weise, Phys. Rev. D **75**, 034007 (2007).
[26] M. Ciminale, R. Gatto, N. D. Ippolito, G. Nardulli, and M. Ruggieri, Phys. Rev. D **77**, 054023 (2008); M. Ciminale, G. Nardulli, M. Ruggieri, and R. Gatto, Phys. Lett. B **657**, 64 (2007).
[27] H. Hansen, W. M. Alberico, A. Beraudo, A. Molinari, M. Nardi, and C. Ratti, Phys. Rev. D **75**, 065004 (2007).
[28] C. Sasaki, B. Friman, and K. Redlich, Phys. Rev. D **75**, 074013 (2007).
[29] B. -J. Schaefer, J. M. Pawlowski, and J. Wambach, Phys. Rev. D **76**, 074023 (2007).
[30] P. Costa, C. A. de Sousa, M. C. Ruivo, and H. Hansen, arXiv:0801.3616; P. Costa, M. C. Ruivo, C. A. de Sousa, H. Hansen, and W. M. Alberico, arXiv:0807.2134.
[31] K. Kashiwa, H. Kouno, M. Matsuzaki, and M. Yahiro, Phys. Lett. B **662**, 26 (2008).
[32] W. J. Fu, Z. Zhang, and Y. X. Liu, Phys. Rev. D **77**, 014006 (2008).
[33] H. Abuki, M. Ciminale, R. Gatto, G. Nardulli, and M. Ruggieri, Phys. Rev. D **77**, 074018 (2008); H. Abuki, M. Ciminale, R. Gatto, N. D. Ippolito, G. Nardulli, and M. Ruggieri, Phys. Rev. D **78**, 014002 (2008); H. Abuki, R. Anglani, R. Gatto, G. Nardulli, and G. Nardulli, Phys. Rev. D **78**, 034034 (2008).
[34] Y. Sakai, K. Kashiwa, H. Kouno, and M. Yahiro, Phys. Rev. D **77**, 051901(R) (2008); **78**, 036001 (2008).
[35] Y. Sakai, K. Kashiwa, H. Kouno, M. Matsuzaki, and M. Yahiro, Phys. Rev. D **78**, 076007 (2008).
[36] A. Roberge and N. Weiss, Nucl. Phys. **B275**, 734 (1986).
[37] J. D. Walecka, Ann. Phys. (N.Y.) **83**, 491 (1974).
[38] T. Kashiwa and T. Sakaguchi, Phys. Rev. D **68**, 065002 (2003).
[39] H. Kouno, T. Sakaguchi, K. Kashiwa, M. Hamada, H. Tokudome, M. Matsuzaki, and M. Yahiro, Soryushiron Kenkyu **112**, C67 (2005).
[40] F. Karsch, Lect. Notes Phys. **583**, 209 (2002).
[41] F. Karsch, E. Laermann, and A. Peikert, Nucl. Phys. **B605**, 579 (2001).
[42] M. Kaczmarek and F. Zantow, Phys. Rev. D **71**, 114510 (2005).
[43] G. Boyd, J. Engels, F. Karsch, E. Laermann, C. Legeland, M. Lütgemeier, and B. Petersson, Nucl. Phys. **B469**, 419 (1996).
[44] O. Kaczmarek, F. Karsch, P. Petreczky, and F. Zantow, Phys. Lett. B **543**, 41 (2002).
[45] V. Bernard, U. G. Meissner, Nucl. Phys. **A489**, 647 (1988).
[46] S. Ejiri, Phys. Rev. D **77**, 014508 (2008); **78**, 074507 (2008).